Journal of Biomedical Optics

SPIEDigitalLibrary.org/jbo

Scanning two-photon microscopy with upconverting lanthanide nanoparticles via Richardson-Lucy deconvolution

Christian F. Gainer
Urs Utzinger
Marek Romanowski

SPIE

Scanning two-photon microscopy with upconverting lanthanide nanoparticles via Richardson-Lucy deconvolution

Christian F. Gainer, Urs Utzinger, and Marek Romanowski
The University of Arizona, Department of Biomedical Engineering, Tucson, Arizona, 85721-0240

Abstract. The use of upconverting lanthanide nanoparticles in fast-scanning microscopy is hindered by a long luminescence decay time, which greatly blurs images acquired in a nondescanned mode. We demonstrate herein an image processing method based on Richardson-Lucy deconvolution that mitigates the detrimental effects of their luminescence lifetime. This technique generates images with lateral resolution on par with the system's performance, ~1.2 μm, while maintaining an axial resolution of 5 μm or better at a scan rate comparable with traditional two-photon microscopy. Remarkably, this can be accomplished with near infrared excitation power densities of 850 W/cm^2, several orders of magnitude below those used in two-photon imaging with molecular fluorophores. By way of illustration, we introduce the use of lipids to coat and functionalize these nanoparticles, rendering them water dispersible and readily conjugated to biologically relevant ligands, in this case epidermal growth factor receptor antibody. This deconvolution technique combined with the functionalized nanoparticles will enable three-dimensional functional tissue imaging at exceptionally low excitation power densities. [DOI: 10.1117/1.JBO.17.7.076003]

Keywords: upconversion; nanoparticle; two-photon microscopy; lanthanide; optical sectioning.

Paper 12169 received Mar. 9, 2012; revised manuscript received May 22, 2012; accepted for publication May 24, 2012; published online Jul. 6, 2012.

1 Introduction

In recent years, there have been numerous advances in the development and use of upconverting lanthanide nanoparticles (UNPs) for biomedical imaging.[1,2] These efforts are driven by the increasing need for improved contrast agents and robust sensors for advanced imaging modalities such as multiphoton and super-resolution microscopy.[3,4] Of particular interest are $NaYF_4$ nanocrystals, chosen for their low phonon energy, codoped with a combination of trivalent lanthanide ions, commonly Yb^{3+} and either Er^{3+} or Tm^{3+}.[5] UNPs have numerous advantages over more traditionally used molecular fluorophores. Excitation of these particles typically takes advantage of the $^2F_{7/2} \rightarrow {}^2F_{5/2}$ transition in Yb^{3+} ions at 980 nm. Energy transfer from these sensitizers to other nearby Ln^{3+} ions can cause multiple excitation steps, culminating in anti-Stokes shifted emission. As a result, autofluorescence, a significant contributor to unwanted background signal in fluorescence imaging, is absent. In addition, UNPs are extremely photostable, and exhibit almost no loss in luminescence after long periods of illumination except at very high excitation powers.[6,7] Energy transfer upconversion (ETU), the mechanism by which these particles are excited, is very efficient when compared to other multiphoton excitation processes, in part because it makes use of real intermediate electronic states during excitation. As an example, ETU is as much as ten orders of magnitude more efficient than two-photon absorption without a real intermediate electronic state in similar materials (Fig. 1).[8]

Address all correspondence to: Marek Romanowski, The University of Arizona, Department of Biomedical Engineering, 1657 E Helen St, Tucson, Arizona, 85721-0240. Tel: 520-626-1578; Fax: 520-626-4824; E-mail: marekrom@email.arizona.edu.

These properties make a compelling case for the use of UNPs as exogenous contrast agents for two-photon scanning microscopy. The relationship between excitation power and emission intensity is still quadratic for two-photon ETU, leading to optical sectioning similar to two-photon microscopy with endogenous fluorophores.[9] While ETU is very efficient when compared to other forms of multiphoton excitation, it is still considerably less efficient at producing light than single photon processes. Quantum yields for $NaYF_4$:Yb^{3+}, Er^{3+}(Tm^{3+}) are typically between 0.005% and 3%.[10] The electronic transitions that result in lanthanide luminescence typically occur within the 4f orbital of these ions, and are consequently forbidden. An immediate consequence of this property is that the absorption cross-sections of lanthanide ions are relatively small. The highly sensitive detection obtained with two-photon scanning microscopy techniques helps to mitigate these properties.

Another consequence of these luminescent transitions being forbidden is that the luminescence lifetime of excited UNPs is long; lifetimes greater than 100 μs are not uncommon. This has advantages in some applications, particularly those that sense changes in the local environment by measuring changes in the luminescence lifetime.[11–15] However, this long lifetime is a hindrance when imaging with a fast scanning microscopy technique, with a pixel dwell time as short as 1 μs. For a pixel dwell time less than 500 μs, nanoparticle emission is streaked along the fast-scan axis of the microscope (Fig. 2). This streaking is the result of nanoparticle emission from previously scanned locations being attributed to the current location of the excitation focus. In addition to emission streaking, the long lifetime of Ln^{3+} excited states makes it fairly easy to saturate the first

0091-3286/2012/$25.00

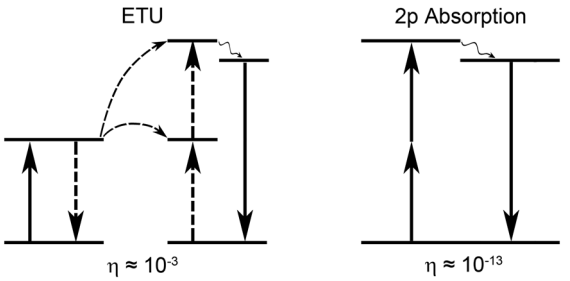

Fig. 1 Diagram of ETU and two-photon absorption with efficiencies for each process in lanthanide materials.[8] Solid arrows represent absorption and emission of light. Dashed arrows represent nonradiative population and depopulation processes that are caused by energy transfer between two lanthanide ions. The wavy arrow represents internal conversion.

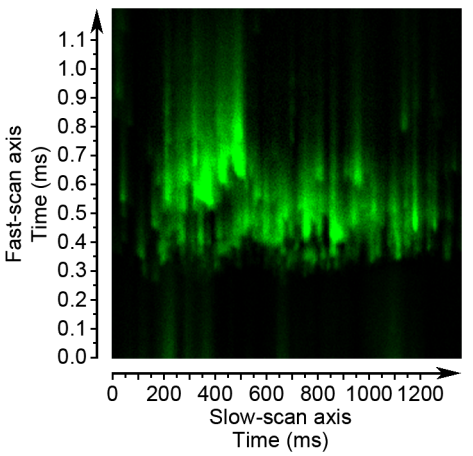

Fig. 2 A demonstration of the streaking observed by two-photon scanning microscopy when contrast agents with long luminescence lifetimes are used. The image is of 665 nm emission from lipid coated $NaYF_4$: Yb^{3+}, Er^{3+} nanoparticles following 980 nm excitation. The fast-scan axis represents the direction of a single line acquisition, with lines added sequentially in the direction of the slow scan axis. Long-lasting luminescence collected in nondescanning mode obscures the actual distribution of luminescent nanoparticles. In this example, the pixel dwell time was 4.6 μs per pixel and the luminescence lifetime is approximately 358 μs.

step of the ETU excitation process. This saturation results in a change in the relationship between emission intensity and excitation power, from quadratic to linear, for many of the emission lines in UNPs.[7] In essence, excitation of UNPs begins to behave like a single photon process and optical sectioning is lost.

These now recognized characteristics of UNPs obscure their potential as robust and efficient contrast agents for advanced imaging modalities based on laser scanning. Both Li's and van Veggel's groups have reported on these issues previously, and each has developed a working solution to mitigate some of the effects of a long luminescence lifetime at the expense of, respectively, light throughput and optical sectioning.[16,17] In addition, Faris's group has addressed a similar issue in multiphoton imaging with europium chelates.[18] In spite of these efforts, applications of UNPs in biomedical imaging remain limited, with the bulk of data generated to date obtained by wide field imaging techniques.[1,6]

Herein, we report an image processing method for mitigating the effects of this long luminescence lifetime on lateral resolution while preserving a short pixel dwell time and low excitation power, both of which are essential for rapid acquisition of luminescence images while maintaining optical sectioning. This method employs Richardson-Lucy (R-L) deconvolution by the time resolved luminescence of UNP emission in order to remove pixel streaking, resulting in images with roughly equivalent resolution in the fast-scan and slow-scan axes of a two-photon scanning microscopy image. As proof of principle for the application of deconvolution to this specific problem, $NaYF_4$: Yb^{3+}, Er^{3+} nanoparticles were synthesized by thermal decomposition, rendered water compatible by lipid coating, and functionalized with an antibody for epidermal growth factor receptor (anti-EGFR). Following functionalization, these UNPs were incubated with 12-μm-thick sections of mouse ear tissue, which is known to express EGFR, and imaged using a two-photon scanning microscopy system.

2 Methods/Materials

2.1 *Nanoparticle Synthesis*

All reagents used in synthesis were obtained from Sigma-Aldrich. $NaYF_4$: Yb^{3+}, Er^{3+} nanoparticles were synthesized by a thermal decomposition method described in several publications.[19–21] In a typical synthesis, 2 mmol of $LnCl_3$ at a molar ratio of 78:20:2 Y^{3+}:Yb^{3+}:Er^{3+} were added to 11 mL of oleic acid and 30 mL of 1-octadecene. The solution was purged of oxygen and water by alternating between vacuum and Ar flow while heating slowly to 150°C. The solution remained at 150°C for 30 min, and was subsequently cooled to 50°C. About 5 mmol of NaOH and 8 mmol of NH_4F were added to 20 mL of methanol. This solution was then slowly added to the reaction vessel over the course of 20 min under Ar flow. The resulting cloudy mixture was kept at 50°C for 30 min, at which time any remaining methanol was removed by vacuum and heat. The solution was then heated to 300°C at ~10°C per min and was held at that temperature for 90 min in Ar atmosphere. Nanoparticles were precipitated by addition of 60 mL of ethanol once the solution had cooled to room temperature, and then separated by centrifugation at 1000 g. The supernatant was discarded and the pellet was redispersed in minimal dichloromethane, then washed several times with excess ethanol. As synthesized, these nanoparticles were hydrophobic.

2.2 *Lipid Coating*

To render particles water compatible, a novel coating method was employed. Fifty milligrams of UNPs were dried with lipids at two times the concentration necessary to coat each particle once. DPPC, DPPE-[methoxy(PEG)2000], and DSPE-[carboxy(PEG)2000] (Avanti Polar Lipids, Alabama) were used at a molar ratio of 95:4.5:0.5 DPPC:DPPE:DSPE. Once dried, 1.2 mL of MES buffer was added to the mixture of lipids and UNPs and heated to 50°C. Particles were dispersed via sonication and filtered multiple times through a series of Nucleopore polycarbonate membranes (Whatman, Kent, United Kingdom) with decreasing size cutoffs. These particles were then functionalized with anti-EGFR.

2.3 *Bioconjugation to Anti-EGFR*

6.5 mg N-hydroxysulfosuccinimide, 5.31 μL N-(3-dimethylaminopropyl)-N'-ethylcarbodiimide, and 235 μL of deionized water were added to 300 μL of the coated particles in

10 mM MES. After 10 min of gentle stirring at room temperature, 30.6 μg of anti-EGFR rabbit polyclonal IgG (Santa Cruz Biotechnology, California, USA) were added. The solution was stirred overnight at 4°C. Purification was by dialysis against DI water with a 300 kDa membrane cutoff. Following dialysis, the presence of bound anti-EGFR was confirmed by the presence of a UV absorption peak at ~280 nm. Particles were used for tissue staining and subsequent imaging immediately following purification.

2.4 *Nanoparticle Characterization*

$NaYF_4:Yb^{3+}$, Er^{3+} nanoparticles were sized by quasi-elastic light scattering using a ZS-90 Zetasizer (Malvern, Worcestershire, United Kingdom). Emission spectra were measured by a QE65000 back-thinned CCD spectrometer (Ocean Optics, Florida, USA) using a 980 nm laser diode for excitation. Luminescence decays were measured by a single photon counting avalanche photodiode (PerkinElmer, Vaudreuil, Québec, Canada) and multichannel scaler (Picoquant, Berlin, Germany) using a tunable optical parametric oscillator (OPO) pumped by a Nd:YAG laser Q-switched at 20 Hz with a 3 ns pulse width for excitation. Luminescence rise and decay constants were determined by fitting lifetime data to $-\mathrm{A}e^{-t/\tau 1} + \mathrm{B}e^{-t/\tau 2} + \mathrm{BKG}$, where $\tau 1$ is the rise constant and $\tau 2$ is the decay constant.

2.5 *Tissue Staining*

To prepare tissue for imaging, a mouse was euthanized with CO_2 and ear tissue was removed and fixed in Histochoice (AMRESCO, Ohio). Fixed ear tissue was embedded in paraffin and sectioned at 12 μm. Sections were deparaffinized and rehydrated to water. Phosphate buffered saline was added to the suspension of purified particles to achieve an osmolality of 286 mmol/kg. Each tissue section was then incubated with approximately 100 μL of the anti-EGFR-UNPs at 4°C for approximately 16 h.[22] The slides were then washed with DI water and mounted with cover slips for imaging.

2.6 *Two-Photon Scanning Microscopy*

Two-photon scanning microscopy was carried out using a Ti:Sapphire laser with ~100 fs pulse width and a repetition rate of 80 MHz for excitation and a commercial laser scanning microscope (LaVisionBiotec, Bielefeld, Germany). All images were collected using a 20X water immersion objective lens with a NA of 0.95. Emission from the nanoparticles was collected at 665 nm following 980 nm excitation. Tissue autofluorescence was collected at 460 nm following 780 nm excitation. Both channels were detected using H7442A-40 PMTs (Hamamatsu Photonics, Hamamatsu City, Japan). Excitation power density was determined by measuring average power at the sample and dividing by the area of a circle with a 1 μm radius. For reference, a 15.4 mW average power measured at the sample is equivalent to ~490 kW/cm^2. Images were processed by background subtraction followed by deconvolution with a PSF determined by the exponential rise and decay of lipid coated UNPs. Deconvolution was performed by a custom script developed in MATLAB (MathWorks, Massachusetts) using the R-L function.[23,24] The axial resolution was assessed at varying excitation power densities. Image stacks were generated for a single particle bound to a glass slide and were composed of 81 images covering 40 μm in depth at 0.5 μm steps and the FWHM was measured from the axial profiles of these image stacks. Images used in this analysis were 255 by 255 pixels and had a pixel dwell time of 19.6 μs. The lateral field of view was 100 μm in both dimensions.

3 Results and Discussion

3.1 *Nanoparticle Characterization*

Following synthesis, $NaYF_4:Yb^{3+}$, Er^{3+} nanoparticles had an average number weighted diameter of approximately 60 nm. Once lipid coated, these UNPs had an average diameter of ~60 nm and were easily dispersed in water, indicating that the bulk of the nanoparticles were coated by a single monolayer. The size distribution had a full width half max of 11.5 nm. While an increase of ~4 nm in diameter is expected following the addition of a lipid monolayer, this change was not detectable with the particle sizer used. Following conjugation to anti-EGFR and subsequent purification of the sample by dialysis, a UV absorption peak at ~280 nm was observed, verifying the presence of anti-EGFR attached to nanoparticles. Luminescence decay profiles were collected for uncoated and coated particles. The red emission from uncoated particles in dichloromethane was fit by the exponential rise and decay described previously with a rise constant of 75.2 μs and a decay constant of 348.9 μs. This fit had a reduced χ^2 of 1.62. Fitting the luminescent decay of red emission from the lipid coated UNPs to the same equation resulted in a rise constant of 23.8 μs and a decay constant of 358.3 μs, with a reduced χ^2 of 1.11 (Fig. 3).

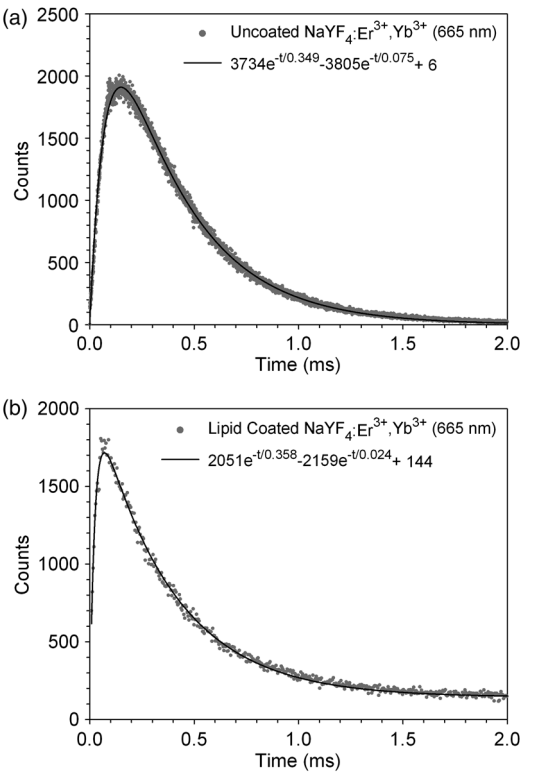

Fig. 3 Time-resolved luminescence of $NaYF_4:Yb^{3+}$, Er^{3+} nanoparticles following excitation by a 3 ns laser pulse at 980 nm. (a) Rise and decay of red emission from uncoated particles in dichloromethane. A bin width of 2.048 μs was used. (b) Rise and decay of red emission from lipid coated particles in MES. A bin width of 4.096 μs was used.

3.2 *Optical Sectioning with UNPs*

In order to determine an excitation power density that would maximize emission intensity while retaining optical sectioning, we investigated the effect excitation power density has on axial resolution. For the measurements shown in Fig. 4, a dwell time of 19.6 μs per pixel was used. As can be seen in Fig. 4, as excitation power density is decreased from 490 kW/cm^2 to 850 W/cm^2, the axial resolution improves from a full width half maximum (FWHM) of 37 μm to approximately 5 μm. Using this information, we chose an excitation power density of approximately 21 kW/cm^2 for our imaging experiments, which corresponds with an axial FWHM of 7 μm.

3.3 *Richardson-Lucy Deconvolution*

The images in Fig. 5 were collected using a scan speed of 200 lines per second, a 510 by 510 pixel resolution, and a 400 μm field of view. The resulting dwell time was 9.23 μs per pixel. The image shown in Fig. 5(a) was obtained by summing eight images acquired at this scan speed, resulting in a total image acquisition time of 18.7 s. Due to the long luminescence decay time of nanoparticle emission at 665 nm, the resulting luminescence image is heavily streaked along the fast-scan axis of the image. This streaked image can be represented as the convolution of the true image with the exponential rise and decay of UNP luminescence,

$$g(x,y) = f(x,y) \otimes h(x,y) + n(x,y), \tag{1}$$

where g is the blurred luminescence image, f is the true image that we wish to resolve, $\otimes$ is the convolution operator, n is noise, x and y are positions along the slow-scan and fast-scan axes respectively, and the PSF is described by

$$h(x,y) = \left(-\mathrm{A}e^{\frac{-y}{v\tau 1}} + \mathrm{B}e^{\frac{-y}{v\tau 2}}\right) \int \delta(x)\mathrm{d}x, \tag{2}$$

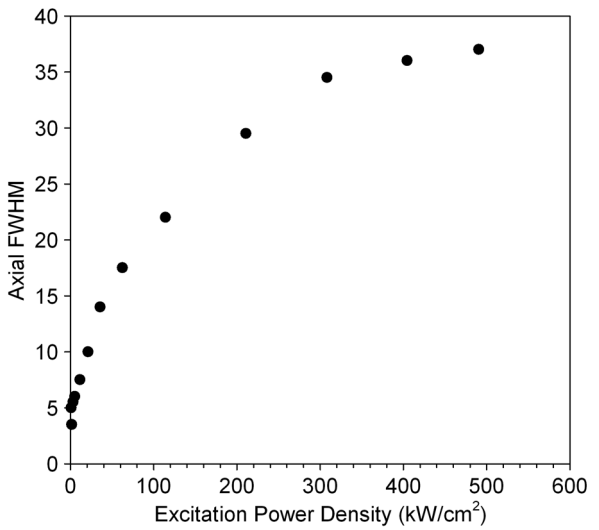

Fig. 4 Axial resolution versus excitation power. Axial resolution was determined by imaging emission from a single, lipid coated nanoparticle at 0.5 μm steps for 40 μm along the z-axis. Images used were 255 by 255 pixels, and were taken with a 19.6 μs dwell time. The field of view used was 100 μm by 100 μm. Excitation power was calculated assuming a 1 μm radius spot size. The axial FWHM of the system was measured as ~2.5 μm.

where $\delta(x)$ is a Dirac delta along the slow-scan axis and v is the fast-scan speed. In trying to solve this equation for f, we are fortunate because we can easily determine the parameters of this point spread function (PSF) with single photon counting. However, even with a known PSF, it is difficult to resolve the true image using a simple linear inverse filter due to the presence of significant photon noise, especially at the tail of nanoparticle emission. Instead, we apply an iterative deconvolution technique to retrieve our desired image. R-L deconvolution is an iterative deconvolution technique that is well known in the astronomy and medical imaging communities and is commonly used to resolve blurred images generated in the presence of significant Poisson distributed noise. R-L deconvolution is described by

$$\hat{f}_{(k+1)} = \hat{f}_{(k)}\left(h * \frac{g}{h \otimes \hat{f}_{(k)}}\right), \tag{3}$$

where $f_{(k)}$ is the estimated image after k iterations and $*$ is the correlation operator.[25] This iterative method almost always converges; however, it is usually unwise to iterate to convergence, as the deconvolution begins to amplify noise after many iterations.

Figure 5 conveys the result of the deconvolution we employed to resolve streaked images. Because the distortion from luminescence lifetime is entirely one dimensional, we can separate the image into single pixel slices along the fast-scan axis. Figure 5(b) plots the profile of one such section, from which it can be observed that nanoparticle emission matches well with the fit obtained through single photon counting in a suspension of lipid coated UNPs. R-L deconvolution of these profiles typically converged after 120 iterations, but between 20 and 60 iterations were sufficient to fully resolve UNPs at a lateral resolution roughly equivalent to that of the slow-scan axis (Figs. 6 and 7). The profile plotted in Fig. 5(c) is the result of 60 iterations of deconvolution. The final, reassembled image is shown in Fig. 5(d).

4 Discussion

Immediately following coating and conjugation, very little aggregation of the UNPs was observed, as indicated by sizing. Over the course of weeks, some settling occurred in lipid coated UNP samples. For particles coated with 50% PEG-lipid instead of the 5% used here, suspensions have remained stable for over one year. As can be seen in Fig. 5, some aggregation of particles did occur during staining of tissue sections. This manifests as differences in intensity between each discrete cluster of particles. A smaller concentration of PEG-lipid in the UNP coating was chosen to avoid interference with conjugation to anti-EGFR and binding to EGFR in the tissue sample; however, a higher concentration may be preferable to prevent this aggregation.

It is interesting to note that while we observe a significant decrease in the rise component of red luminescence, the decay is relatively unchanged by lipid coating and dispersion in an aqueous medium. This discrepancy is likely the result of a match between short-lived excited states in Er^{3+} and high-energy vibrational modes in either the solvent or lipid coating, resulting in preferential quenching of those states.[26] While the contribution of individual time constants to each decay component is complex, increased quenching of the $^4S_{3/2}$ or $^4F_{9/2}$ excited states may explain the observed effect.[27]

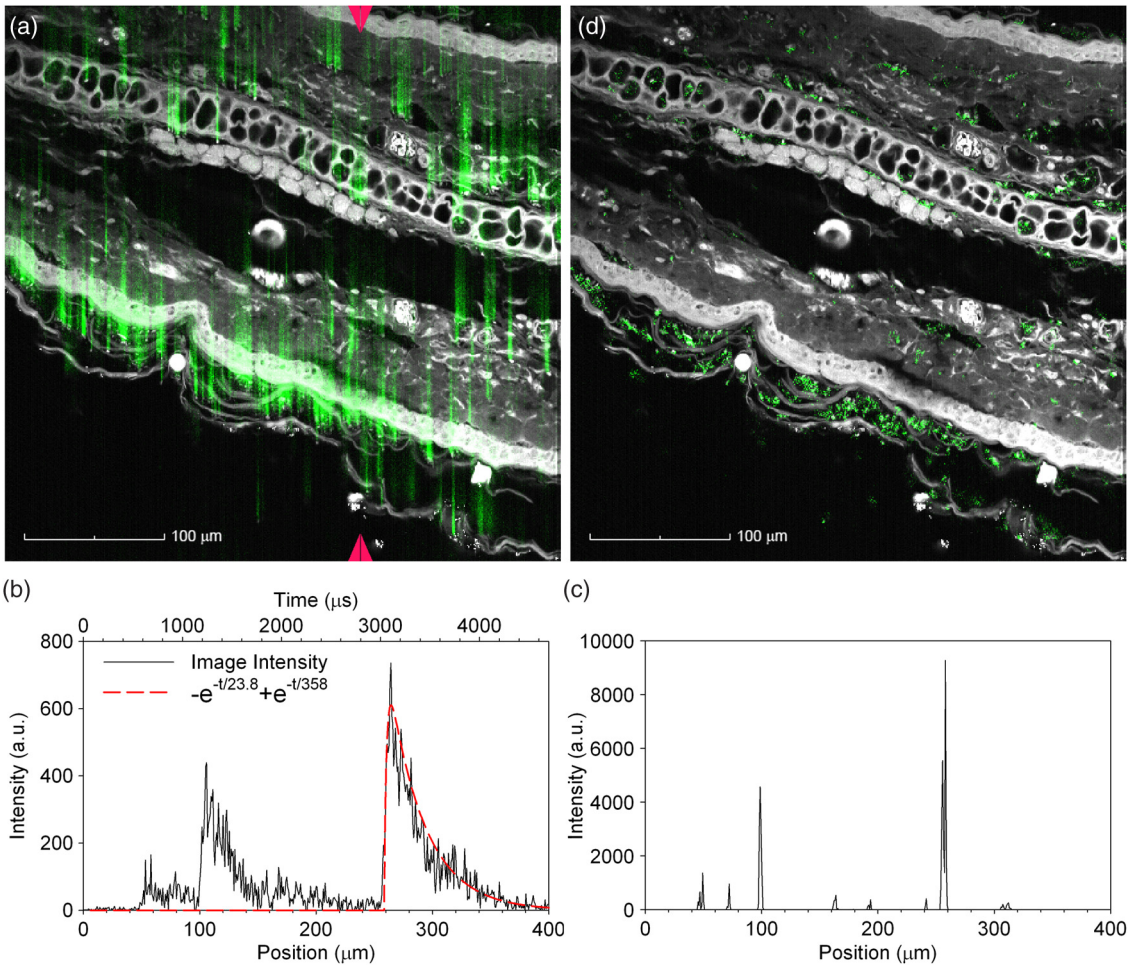

Fig. 5 A 12-μm section of murine ear stained with anti-EGFR-$NaYF_4$:Yb^{3+}, Er^{3+} nanoparticles, false colored green here. The grayscale images shown are tissue autofluorescence at 460 nm following 780 nm excitation. UNP emission was collected at 665 nm following 980 nm excitation. Images were 510 by 510 pixels and represent a 400 μm field of view. Dwell time was 9.2 μs per pixel. The excitation power density was 21 kW/cm^2 for the upconversion luminescence image and ~10 MW/cm^2 for the autofluorescence image. (a) Full image before deconvolution. The arrows at top and bottom represent the location of the profile shown in (b). (b) Profile taken along a single scan line of an image of upconverting nanoparticles bound to tissue. The dashed line is equivalent to the PSF used for deconvolution, shifted and scaled to overlap with the rise and decay of a single particle. PSF amplitudes were set equal for simplicity. (c) The same profile following deconvolution with the PSF shown in the left image. This profile is the result obtained following 60 iterations of R-L deconvolution. (d) Full image after deconvolution of each line along the fast-scan axis.

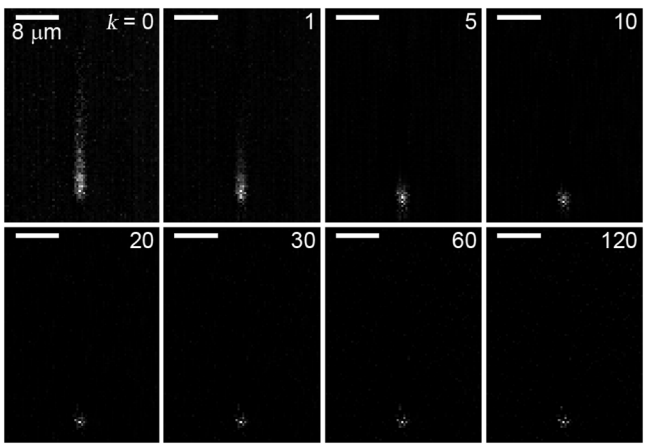

Fig. 6 Deconvolution of luminescence from a single, lipid coated nanoparticle over 120 iterations. Excitation power density for these images was ~850 W/cm^2. Iteration number is shown in the top right of each image. Images were normalized to the same maximum value for comparison purposes.

The method of image acquisition presented here compares very favorably to the methods recently proposed by the Li and van Veggel groups.[16,17] In the former, a confocal pinhole was added to the image acquisition path in order to block out of focus light.[16] This has the advantage of improving axial resolution at high excitation powers and is successful in removing pixel bleeding caused by UNP emission. However, this method is not without disadvantages. UNP emission typically does not reach a maximum until many microseconds after excitation. If the pinhole is large, peak emission is observed at a location down-scan from the actual nanoparticle location and may include emission from adjacent nanoparticles. If the pinhole is small enough to properly locate the particle, peak emission is ignored altogether and much higher excitation power densities are required in order to detect nanoparticle emission. In addition, removing the tail end of emission also removes UNP sensitivity to dynamic events that interact with the long lived electronic states.

In the latter, a different approach to avoiding UNP emission streaking present in scanning microscopy images is

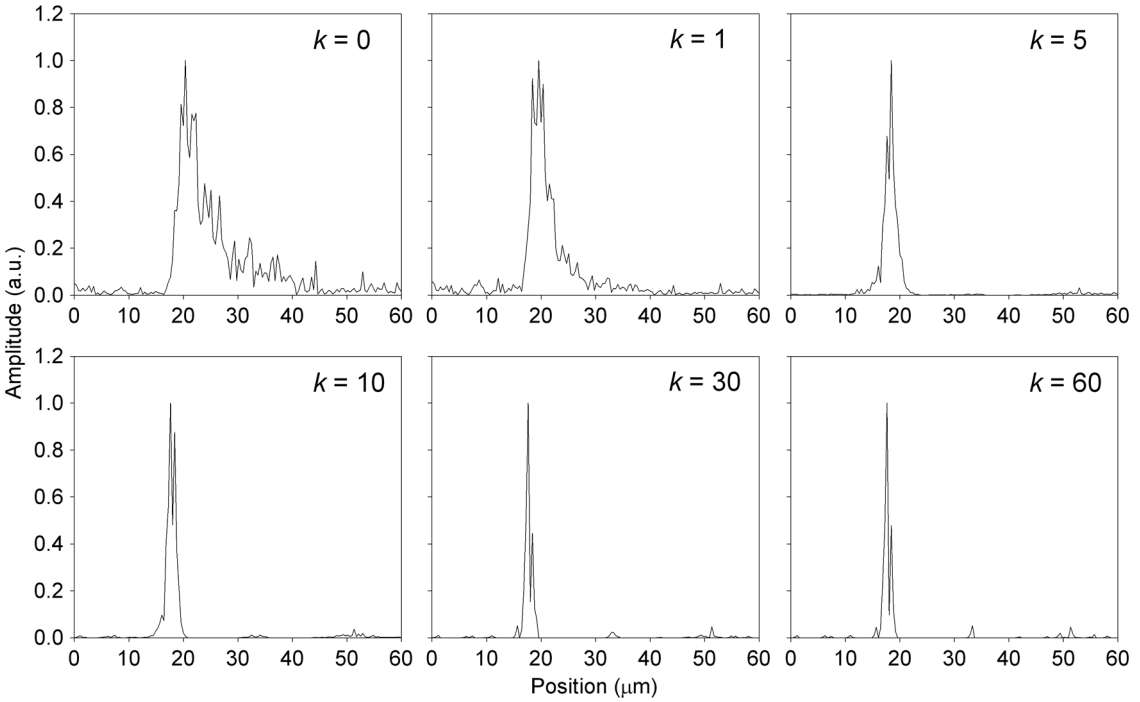

Fig. 7 Single fast-scan line taken from images in Fig. 6 and presented in profile. Intensities are normalized to aid comparison. Excitation power density was ~850 W/cm^2. Iteration number is shown in the top right of each plot.

demonstrated.[17] This approach instead uses wide-field imaging, and is able to associate the entire rise and decay of UNP emission with a specific location that corresponds well with the particle location. There are two immediately apparent drawbacks to this method of imaging when compared to two-photon scanning microscopy. First, scattering of emission light will result in a slight loss of lateral resolution, increasing with depth into a tissue sample. More importantly, wide field illumination prevents the use of this imaging technique as an optical sectioning technique.

Another method for avoiding the streaking effects caused by long lanthanide luminescence was presented by Faris's group.[18] This method replaces the PMT detection typically used for multiphoton microscopy with a CCD camera while retaining scanned excitation. This wide-field acquisition results in images that are free of streaking along the fast-scan axis and have the same potential for optical sectioning as a multiphoton microscopy system. When working in thick tissue samples, wide-field acquisition may, however, result in a loss of lateral resolution due to collection of scattered luminescence photons.

The solution proposed here retains optical sectioning and detects the entire rise and decay of UNP luminescence, maximizing the amount of light collected. R-L deconvolution of images like that shown in Fig. 5 was implemented using a fairly simple script in MATLAB. Sixty iterations of this script completed in ~7 s using an Intel Core2 Duo E7200 CPU at 2.53 GHz. On the other hand, differences in individual nanoparticle lifetimes will result in small differences in the effectiveness of a set number of R-L deconvolution iterations. Because the deconvolution takes Poisson noise into account, it is also possible for signal from a single particle to be mistaken as part of the streaking from a large aggregate of particles located immediately up-scan. These issues can be in part addressed by implementing a goodness-of-fit test to control the iterative process of deconvolution. Further optimization of the R-L deconvolution and a better processor would likely allow for implementation of this method as an unobtrusive part of image acquisition rather than a post-processing step. It may also be possible to parallelize deconvolution and image acquisition to some extent, such that deconvolution begins on each scan line as soon as it is collected, before image acquisition has finished. The use of a software based solution to the problem of UNP streaking is particularly enticing because it allows commercially available two-photon microscopy systems to be used for UNP imaging without hardware modification.

5 Conclusion

We have shown that deconvolution by a point spread function determined by the time resolved luminescence of upconverting nanoparticles can greatly diminish streaking caused by their long lived excited states. R-L deconvolution provides a convenient route to retaining fast image acquisition times and optical sectioning. We have also demonstrated here what we believe to be the first use of lipid coating as a viable method for rendering UNPs water dispersible. In addition, this method of coating provides a convenient platform for conjugation to biologically relevant ligands, as we have demonstrated for anti-EGFR. Further improvements in the quality of these particles, such as the use of a core/shell system,[14] will likely result in better image quality at low excitation power densities. It should also be noted that improvement could be achieved by choosing a different excitation source for two-photon upconversion imaging. While two-photon autofluorescence, associated with femtosecond laser pulses, was minimal at 665 nm, the use of a CW or longer pulse width laser would result in effectively no autofluorescence signal and enable acquisition at all Er^{3+} emission peaks. The detected luminescence intensity could also be increased by using Tm^{3+} instead of Er^{3+}, resulting in a single, large emission

peak at ~800 nm instead of two peaks at 546 and 665 nm. This anti-Stokes shifted NIR emission is also preferred for deep tissue imaging due to its low attenuation in biological samples. This report has focused on the development of a technique to correct the lateral resolution of a two-dimensional (2-D) image of UNPs while maintaining the axial resolution enabled by these contrast agents. Future work will apply lateral deconvolution to resolve details in three-dimensional (3-D) deep tissue imaging with UNPs.

Acknowledgments

The authors would like to acknowledge Faith Rice for providing tissue samples for these experiments. This work was supported by NIH grants EB000809, CA120350, CA109385, and RR023737 as well as the TRIF imaging program at the University of Arizona.

References

1. J. Zhou, Z. Liu, and F. Li, "Upconversion nanophosphors for small-animal imaging," *Chem. Soc. Rev.* **41**(3), 1323–1349 (2012).
2. F. Wang et al., "Upconversion nanoparticles in biological labeling, imaging, and therapy," *Analyst* **135**(8), 1839–1854 (2010).
3. M. Fernández-Suárez and A. Y. Ting, "Fluorescent probes for super-resolution imaging in living cells," *Nat. Rev. Mol. Cell Biol.* **9**(12), 929–943 (2008).
4. H. M. Kim and B. R. Cho, "Two-photon probes for intracellular free metal ions, acidic vesicles, and lipid rafts in live tissues," *Acc. Chem. Res.* **42**(7), 863–872 (2009).
5. S. Heer et al., "Highly efficient multicolour upconversion emission in transparent colloids of lanthanide-doped $NaYF_4$ nanocrystals," *Adv. Mater.* **16**(23–24), 2102–2105 (2004).
6. D. K. Chatterjee, A. J. Rufaihah, and Y. Zhang, "Upconversion fluorescence imaging of cells and small animals using lanthanide doped nanocrystals," *Biomaterials* **29**(7), 937–943 (2008).
7. Y. Wang et al., "Upconversion luminescence of β-$NaYF_4$:Yb^{3+}, Er^{3+} @β-$NaYF_4$ core/shell nanoparticles: excitation power density and surface dependence," *J. Phys. Chem. C* **113**(17), 7164–7169 (2009).
8. F. Auzel, "Upconversion and anti-Stokes processes with f and d ions in solids," *Chem. Rev.* **104**(1), 139–173 (2004).
9. M. Gu, "Image formation in multiphoton fluorescence microscopy," Chapter 11, in *Handbook of Biomedical Nonlinear Optical Microscopy*, B. R. Masters and P. T. C. So, Eds., pp. 266–282, Oxford University Press, Inc., New York, NY (2008).
10. J. C. Boyer and F. C. J. M. van Veggel, "Absolute quantum yield measurements of colloidal $NaYF_4$:Er^{3+}, Yb^{3+} upconverting nanoparticles," *Nanoscale* **2**(8), 1417–1419 (2010).
11. T. Riuttamäki et al., "Decrease in luminescence lifetime indicating nonradiative energy transfer from upconverting phosphors to fluorescent acceptors in aqueous suspensions," *J. Phys. Chem. C* **115**(36), 17736–17742 (2011).
12. L. Stryer, D. D. Thomas, and C. F. Meares, "Diffusion-enhanced fluorescence energy transfer," *Ann. Rev. Biophys. Bioeng.* **11**, 203–222 (1982).
13. C. G. Morgan and A. C. Mitchell, "Prospects for applications of lanthanide-based upconverting surfaces to bioassay and detection," *Biosens. Bioelectron.* **22**(8), 1769–1775 (2007).
14. G. Neurauter, I. Klimant, and O. S. Wolfbeis, "Microsecond lifetime-based optical carbon dioxide sensor using luminescence resonance energy transfer," *Anal. Chim. Acta* **382**(1–2), 67–75 (1999).
15. R. Ali et al., "Upconverting nanoparticle based optical sensor for carbon dioxide," *Sensor Actuat. B-Chem.* **150**(1), 126–131 (2010).
16. M. Yu et al., "Laser scanning up-conversion luminescence microscopy for imaging cells labeled with rare-earth nanophosphors," *Anal. Chem.* **81**(3), 930–935 (2009).
17. J. Pichaandi et al., "Two-photon upconversion laser (scanning and wide-field) microscopy using Ln^{3+}-doped $NaYF_4$ upconverting nanocrystals: a critical evaluation of their performance and potential in bioimaging," *J. Phys. Chem. C* **115**(39), 19054–19064 (2011).
18. X. Xiao et al., "Cell assay using a two-photon-excited europium chelate," *Biomed. Opt. Express* **2**(8), 2255–2264 (2011).
19. Z. Li and Y. Zhang, "An efficient and user-friendly method for the synthesis of hexagonal-phase $NaYF_4$:Yb, Er/Tm nanocrystals with controllable shape and upconversion fluorescence," *Nanotechnology* **19**(34), 345606 (2008).
20. H. S. Qian and Y. Zhang, "Synthesis of hexagonal-phase core-shell $NaYF_4$ nanocrystals with tunable upconversion fluorescence," *Langmuir* **24**(21), 12123–12125 (2008).
21. K. A. Abel, J. C. Boyer, and F. C. J. M. van Veggel, "Hard proof of the $NaYF_4$/$NaGdF_4$ nanocrystal core/shell structure," *J. Am. Chem. Soc.* **131**(41), 14644–14645 (2009).
22. A. M. Winkler et al., "Quantitative tool for rapid disease mapping using optical coherence tomography images of azoxymethane-treated mouse colon," *J. Biomed. Opt.* **15**(4), 041512 (2010).
23. W. H. Richardson, "Bayesian-based iterative method of image restoration," *J. Opt. Soc. Am.* **62**(1), 55–59 (1972).
24. L. B. Lucy, "An iterative technique for the rectification of observed distributions," *Astron. J.* **79**(6), 745–754 (1974).
25. D. S. C. Biggs and M. Andrews, "Acceleration of iterative image restoration algorithms," *Appl. Opt.* **36**(8), 1766–1775 (1997).
26. N. Bogdan et al., "Synthesis of ligand-free colloidally stable water dispersible brightly luminescent lanthanide-doped upconverting nanoparticles," *Nano Lett.* **11**(2), 835–840 (2011).
27. C. F. Gainer et al., "Control of green and red upconversion in $NaYF_4$:Yb^{3+}, Er^{3+} nanoparticles by excitation modulation," *J. Mater. Chem.* **21**(46), 18530–18533 (2011).